Grant Agreement:	**247223**
Project Title:	**A**dvanced **R**adio In**T**erface Technolog**I**es for 4G **S**ys**T**ems ARTIST4G
Document Type:	Deliverable

Document Identifier:	
Document Title:	**D6.2 - Laboratory and field trial results connected to the first set of innovations**
Source Activity:	WP6
Editors:	Michael Grieger and Johannes Koppenborg
Authors:	See table page 3
Status / Version:	final
Date Last changes:	29.09.2011
File Name:	D6p2_final.doc

Abstract:	This deliverable provides a first summary on field trial results and evaluation which can be used as an input into standardization, and contains structured feedback on the concepts themselves

Keywords:	LTE, LTE advanced, CoMP, 2D and 3D Beamforming, channel estimation

Table of Contents

Authors

Name	Beneficiary	E-mail address
Johannes Koppenborg	ALUD	johannes.koppenborg@alcatel-lucent.com
Cornelis Hoek	ALUD	cornelis.hoek@alcatel-lucent.com
Michael Grieger	TUD	michael.grieger@inf.et.tu-dresden.de
Denis Dutoit	CEA	denis.dutoit@cea.fr
Dimitri Kténas	CEA	dimitri.ktenas@cea.fr
Nicolas Cassiau	CEA	nicolas.cassiau@cea.fr
Rabih Chrabieh	SEQ	rchrabieh@sequans.com
Serdar Sezginer	SEQ	serdar@sequans.com

1 Executive Summary

This deliverable summarizes first field trial results of ARTIST4G. In particular, measurements indicate the great potentials of 3D beamforming and show gains of different uplink 'CoMP schemes in a field trial. Furthermore, the current status of the implementation of a downlink CoMP test bed that will be developed on Magali system-on-chip boards is presented and the small-scale implementation of advanced channel estimation algorithms on a LTE compliant UE platform shows that their actual performance matches the simulated prediction.

2 Introduction

The project ARTIST4G has the objective to improve the ubiquitous user experience of cellular mobile radio communication systems by focusing on the following requirements: high spectral efficiency and user data rate across the whole coverage area, fairness between users, low cost per information bit, and low latency. At this point in the project's lifetime, we have seen a series of high quality deliverables and papers that show innovative concepts and by benchmarking them with the state-of-the-art to fulfill the above requirements following one of the concepts: interference avoidance, Interference exploitation, and advanced relay techniques.

A primary feature of ARTIST4G is that theoretical and simulation studies of innovations are accompanied by lab and field trials, which give important input to fine tune and evaluate interesting concepts as we will show in this deliverable on first field trial results. Following this approach we believe that the project will not only have a strong impact on standardisation but is also the birthplace of new ideas that are the results of strong cooperation between theoretical research and practical implementation.

A first feedback on the implementation of all innovations in this first set is given in D6.1. The document also presents the four different hardware platforms that are available within the ARTIST4G project. D6.1 show that different aspects of hardware implementation and field trials can be addressed by using these platforms that range from complexity and power consumption studies of particular algorithms to field trial measurements in a representative test bed.

In this deliverable, we will show a first summary of actual lab and field trial results that again prove the great bandwidth of the work done in the project. Section 3.1 shows a proof of concepts of 3D beamforming in a real world scenario investigating instantaneous channel measurements to several antennas with different downtilts. A simulation study as well as implementation results of a feedback less downlink CoMP concept are presented in Section 3.2. Several activities in ARTIST4G involve the use an LTE-Advanced testbed that consists of a large number of sites distributed in downtown Dresden. In the first half of the project the focus of these activities was put on uplink CoMP. Section 3.3 presents an overview of all results that have been gathered until this point, considering several aspects such as multi-antenna base stations, compression of radio signals, and the impact of downtilt. The small-scale implementation of channel estimation algorithms on a LTE compliant UE platform is studied in Section 3.4. The results are compared to simulations that are done in WP2. They show the feasibility and performance of these algorithms on a state of the art architecture.

3 Lab and Field Trial Results

3.1 Advanced 3D-Beamforming

3.1.1 Introduction

Beamforming requires that multiple antennas are used to form the transmission or reception beam and to increase the signal-to-noise-ratio at the receiver. This technique can both be used to improve coverage and to increase the system spectral efficiency. The increased signal-to-noise-ratio is not only due to a larger gain in the direction of the desired user, but also due to a better control of the spatial interference distribution in the cell. 2D-beamforming is the common assumption whereas 3D antenna pattern are expected to give significant improvements. As already discussed in [Ref 23], simulations have shown that there are 30% gain on average cell throughput for downlink with 3D antenna pattern (including down-tilting) comparing with 2D antenna pattern in LTE Rel-8 system. The 3D antenna pattern was not yet confirmed in large-scale trials or measurement campaigns, and does not very well consider the constraints operators have to adjust downtilts.
Therefore the main target of the 3D Beamforming lab and field trials is to investigate possible improvements of the spectral efficiency and cell edge throughput for one and more terminals. Depending on the cell size and the height of the base station antenna above ground, the main lobe of the vertical pattern is directed towards the ground in the afar part of the cell.

In a first step we have validated the influence of different antenna downtilts at a specific terminal location. For this we have used an antenna array with 4 antenna columns which can be tilted separately. Tests with this arrangement were done in the 1st half-year of 2011.

In a second step we will use an enhanced eNodeB emulator with an antenna array arrangement which allows emulation of vertical beam steering. With this set up we will go for field trials in Stuttgart in a single cell scenario starting 3rd quarter 2011. Furthermore in the Dresden test bed multi site trials with variation of vertical downtilts are planned for the 3rd quarter 2011 to analyse the influence of neighbour cell interference to vertical beam steering.

3.1.2 Test with fixed downtilts

The aim of the trials with different fixed downtilts is to measure the characteristics of the system behaviour in a real outdoor scenario for typical environmental condition. For these tests we have built up a special antenna array with 4 single columns which can be tilted separately. Each single antenna element is fed with signals with dedicated and distinguishable pilots from an Alcatel Lucent eNodeB emulator. With this arrangement we had the possibility to simultaneously measure up to four data streams with a specific radio network analyzer.

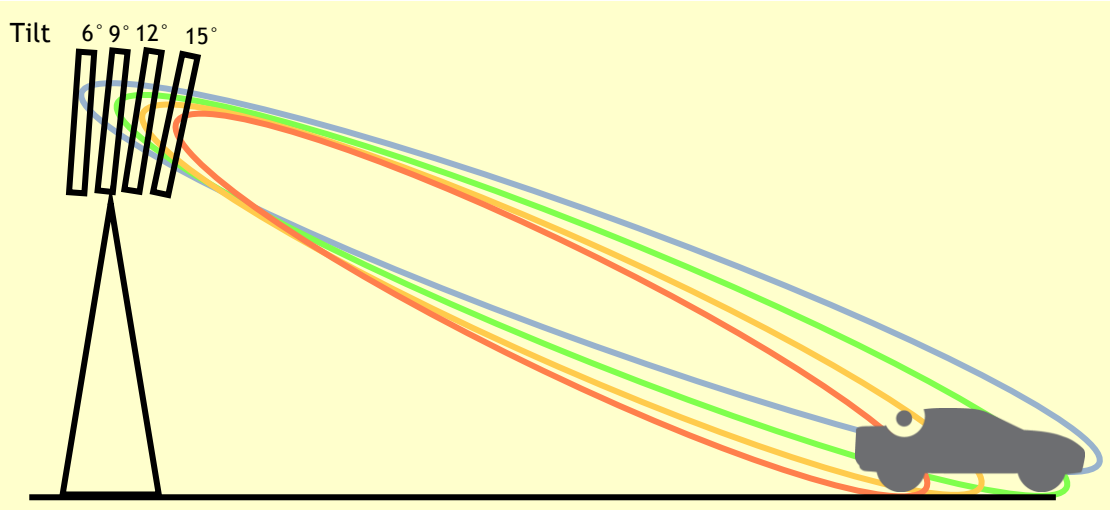

Figure 1 Principle arrangement for simultaneous measurements with different downtilts

The drive routes are chosen in such a way that we could clearly distinguish between regions with mostly line of sight conditions and regions with strong fading conditions.

Figure 2 LTE Testbed in Stuttgart (Source: Open Street View)

Special focus of these trials was the investigation of the impact of different downtilts on the performance metric.

3.1.3 Results and Outlook

Baseline measurements with a downtilt of 6° for all four antenna elements have been done for different drive routes in the Stuttgart test bed. Then test drives were done for different settings of the antenna tilts of the antenna array. The downtilts of the antennas were varied between 0° and 18° with a step size of 3°. The first observation was that fast fading effects hide the impact of different downtilts to the received signal at the terminal device.

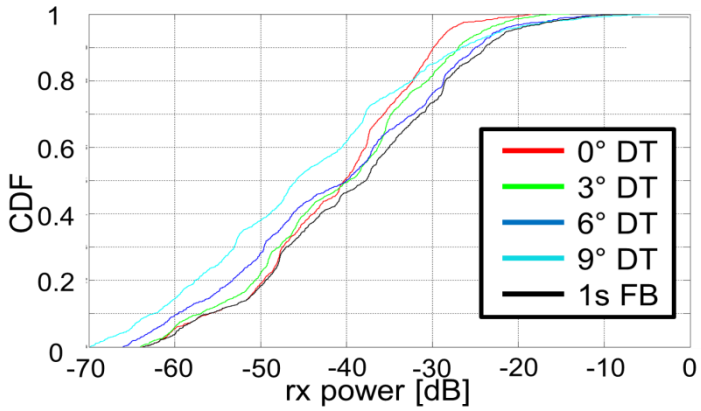

Figure 3 CDF of the Received Power for Downtilts 0°, 3°, 6,° 9° and calculation of optimum downtilt for a feedback loop (FB) with 1 sec delay

Therefore the raw data were integrated over adequate time intervals to neglect the fast fading effects. We observed a slow change of the optimum downtilt for drive test with velocities of up to 20-30 km/h. The variation of the received signals with different downtilts was up to 15 dB which

gives a high potential for a significant throughput gain. The expectation that small tilts will show improved receive signal strength at cell edge and high tilts at cell center could be verified by these measurements quantitatively for this specific deployment scenario. Downtilts > 10° did not show big advantages.

Additional to the single cell trials in Stuttgart the aim of the downtilt tests in the test bed Dresden are to provide an enhanced proof of concept in a typical deployment scenario with several sites.

Test signals with dedicated pilots are sent from the antenna system of the serving cell to a test device installed in a van. The antenna downtilt will be set electrically to tilts between 5° and 17°. Several drive tests with defined downtilts of the serving cell will be done to get a reliable statistic and significant results. In a second step up to 2 surrounding base stations are used as interferer for the serving cell. In a baseline measurement the interference level at the drive route will be measured. Then drive tests will be carried out with tilt variation between 5° and 17° of the serving cell and the neighbour cells to determine the dependency of interference of the serving cell from the downtilt of the interferers. The received signals of the drive tests with and without interference will be analysed taking the topology of the test array into account and compared with the simulation results of WP1. All trials will be done at 2.6 GHz with 6 MHz bandwidth.

For the vertical beamforming trials in Stuttgart we use an adaptive antenna array together with Remote Radio Heads (RRH) and an enhanced eNodeB emulator to run tests with the 3D algorithms. The antenna system for 2.6 GHz, a 4-stacked-XPol antenna, exists of 4 groups of paired XPol dipoles which can be addressed separately. The implementation of the algorithm and the co-operation with RRHs and with test devices has been validated with lab tests. Important for this test was a proper time and phase alignment of the system for each single data link. 3D beamforming field trials in a single cell scenario in Stuttgart in a realistic environment and with one or several test devices are foreseen as proof of concept. Special focus of these 3D beamforming trials will be the impact of different or adapted downtilts per user for the performance metric. The evaluation results of these trials will be compared with our simulations, and depending on the achieved results we will propose improvements of the tested algorithm.

3.2 Downlink CoMP without CSI Feedback

3.2.1 Introduction

Implementation of CoMP concepts on the available hardware platforms will allow validating the theoretical results obtained by simulations. Benefits of CoMP in terms of coverage of high data rates, cell edge throughput and system throughput is investigated by considering real world conditions through lab and field trials. The CEA hardware platform is used for the implementation of DL CoMP Joint Processing without CSI feedback. The MIMO scheme considered here is the double Alamouti (4x2) that combines the robustness of the Alamouti coding with rate doubling ability. Data symbols are separated in two streams, each one using the Alamouti space-time block coding principle on a pair of antennas (a pair of antenna located at each base station).

This particular scheme is being studied in order to assess the improvements in terms of bit rate and robustness, compared to the well-known Alamouti scheme in an interference-limited scenario.

The test of downlink CoMP without CSI feedback is carried out along the project in three implementation steps:

1. Test of 4x2 (double Alamouti) downlink receiver: this first step implements a 4x2 DL receiver.
2. Test of 2x2 downlink: The setup in this intermediate step consists of one UE and one BS implementing a 2x2 downlink scheme and is used as a reference point for performance comparison.
3. Test of virtual double Alamouti: this test consists in implementing a distributed double Alamouti scheme on a test bed composed of two BS and one UE.

In each implementation step, quantitative measurements are performed on the selected algorithms and configurations in order to evaluate the performance in terms of MER, BER, BLER and throughput, especially at the cell edge. The CEA platform also enables specific measurements in terms of complexity and power consumption related to the new algorithms implemented on the Magali ASIC. Processing time and reconfiguration time between modes are also evaluated and delivered as input to WP1-WP2-WP3. These figures of merits are indeed relevant inputs for WP1 since double Alamouti scheme is also studied within WP1 for the uplink scenario (see single cell Double Codeword SU-MIMO/MU-MIMO proposal in section 4.1.4 of D1.2 [18]).

D6.1 [20] provides the implementation feedback connected to the first step and compares expected results from simulations with measurements made on the demonstrator hardware. This D6.2 deliverable aims to describe the simulation set-up and results done as a reference for the hardware implementation step. This deliverable will also provide some implementation feedback on the 2x2 downlink transmitter related to the second implementation step.

Next step is the finalization of the implementation of the user equipment with 2 receives paths followed by the final set-up for the Virtual Double Alamouti Scheme. Performance measurements will be then provided in order to validate the concept of DL CoMP without feedback in the real world.

3.2.2 Simulation results for interference and cooperation scenarios

3.2.2.1 Context of the study

We consider, as shown in Figure 4, two adjacent omni-directional cells, Cell 1 and Cell 2 and their associated eNodeBs, eNodeB1 and eNodeB2 respectively. A UE is positioned on the axis [eNodeB1 eNodeB2] at a distance *d* from eNodeB1. The distance between the two eNodeBs is the Inter Site Distance (ISD).

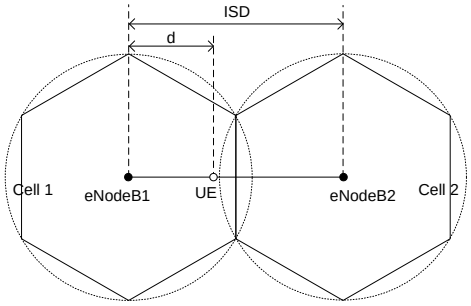

Figure 4: Context of the study

We compare in the following the performance of two scenarios, a scenario with interference (Figure 5) and a scenario with cooperation (Figure 6).

In the first scenario eNodeB1 transmits data to the UE when eNodeB2 is interfering. eNodeB1 and eNodeB2 are equipped with two transmit antennas and perform Alamouti space-time block coding [15]. The UE is equipped with two receive antennas and performs classical Alamouti decoding on each receive antenna followed by an MRC recombination of the signals from the two antennas.

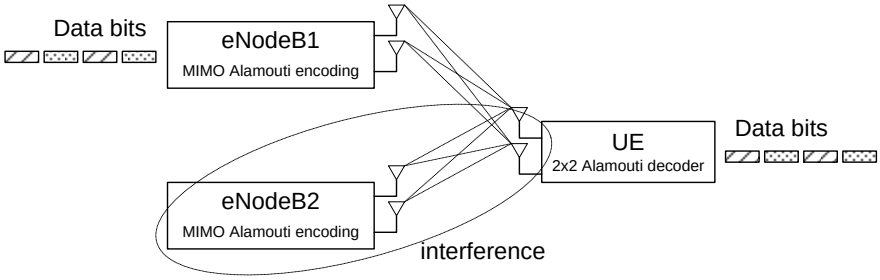

Figure 5: Interference scenario

In the second scenario eNodeB1 and eNodeB2 are cooperating to transmit data to the UE. Data bits are split in two streams, each one using the Alamouti space-time block coding principle on a pair of antennas (a pair of antenna located at each eNodeB), as shown in Figure 6. The UE is equipped with two receive antennas and performs double Alamouti (4x2) decoding with ZF equalization. The double Alamouti decoder combines the robustness of the Alamouti coding with rate doubling ability [21].

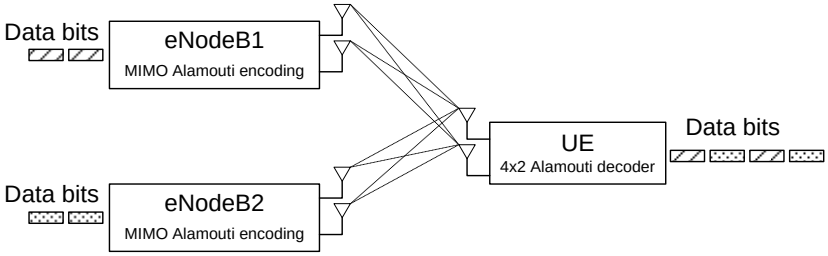

Figure 6: Cooperation scenario

Important note: The data rate between (eNodeB1, eNodeB2) and the UE in cooperation scenario is twice the data rate between eNodeB1 and the UE in interference scenario. Nevertheless, in the first case two eNodeBs are serving one UE with rate 2 and in the second case two eNodeBs are serving two UEs (the interfering eNodeB2 serves a user in Cell 2) with rate 1. So we consider that the maximum achievable global throughput is the same in the two scenarios.

3.2.2.2 Simulator description

Details of the software simulator are presented in Figure 7. Data bits go through the channel coding module. They are then interleaved and mapped into constellation symbols. Those symbols are MIMO encoded thanks to Alamouti scheme. The two resulting streams of symbols are then treated independently.

They are mapped into resource blocks by the chunk mapping module. The framing module then adds guard carriers and DC carrier to build OFDM symbols and complete the frame by introducing OFDM pilot symbols. In the cooperation scenario the pilots dedicated to the estimation of the channel from eNodeB1 to UE are mapped on different carriers than the pilots dedicated to the estimation of the channel from eNodeB2 to UE, so that the UE can estimate all the channels. In the interference scenario, the pilots dedicated to the estimation of the channel from eNodeB1 to UE are interfered by data from eNodeB2.

Finally the IFFT is applied to OFDM symbols and data go through MIMO channel. Fast fading channel is modelled by urban macro 3GPP Spatial Channel Model (SCM) [16] with omnidirectional antennas at the eNodeBs.

At the UE side the inverse operations are done. In the interference scenario the MIMO decoder is the classical Alamouti decoder whereas in the cooperation scenario the MIMO decoder is the double Alamouti decoder. Bit Error Rate (BER) and Frame Error Rate (FER) are evaluated at the output of the channel decoder.

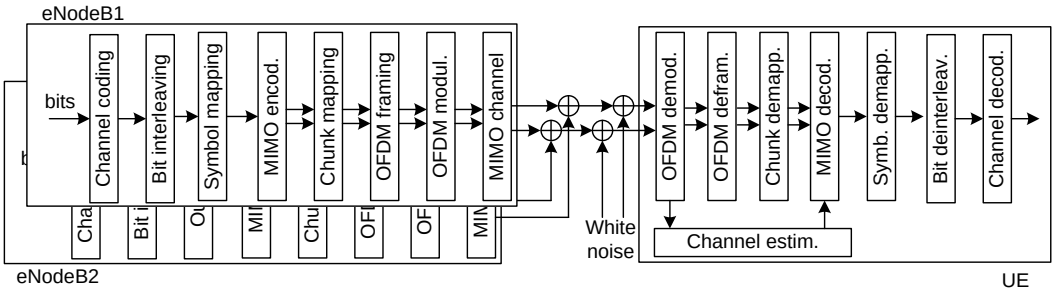

Figure 7: Software simulator

Table 1 presents the parameters of the simulator for the 3 modes considered in the following.

Table 1: Parameters of the simulator

	Mode 1	Mode 3	Mode 5
Nb OFDM symbols per frame	14		
Nb data OFDM symbols per frame	10		
FFT size	1024		
Nb useful carriers	600		
Nb bits per modulation symbol	2	4	6
Nb users	50	25	5
Nb Resource Blocks per user	1	2	10
Equalization	ZF		
Channel coding	Duo-binary turbo codes		
Coding rate	1/2	2/3	3/4
Channel estimation	Frequency filtering + time interpolation		

3.2.2.3 Path loss and SNR computation

The Path Loss (*PL*) between eNodeBs and the UE is Non Line Of Sight (NLOS). It is computed in dB thanks to :

$$PL(d) = PLE_{NLOS} \times \log_{10}\left(\frac{d}{1000}\right) + PLC_{NLOS},$$

where PLE_{NLOS} and PLC_{NLOS} are given in Table 2 and d is the distance between the eNodeB and the UE in meters.

We are then able to compute the Signal to Noise Ratio (SNR) at the input of the ADC (Analog Digital Converter) of the UE as a function of the distance d :

$$SNR(d) = P_{Tx} + G_{Tx} - L_C + G_{Rx} - PL(d) - (NF + L_I + N_T)$$

Table 2 presents the parameters values for SNR computation.

Table 2: Parameters for SNR computation

Transmitter			
Bw	Bandwidth	10	MHz
P_{Tx}	Power at power amplifier output	46	dBm
G_{Tx}	Antenna gain	18	dBi
L_C	Cable loss	2	dB
Channel			
F_c	Carrier Frequency	2	GHz
PLE_{NLOS}	Path loss exponent for NLOS [17]	42.8	
PLC_{NLOS}	Path loss const. for NLOS [17]	151.1*	dB
N_T	Thermal noise	-104	dBm
Receiver			
G_{Rx}	Antenna gain	0	dBi
L_I	Implementation loss	5	dB
NF	Noise figure	8	dB

* including 20 dB penetration loss

3.2.2.4 Simulation results

In all the simulations, the power of the additive white Gaussian noise is set to 0 dB. Then, for each distance *d* a simulation is run with *transmit power*(eNodeB1) = *SNR(d)* and *transmit power*(eNodeB2) = *SNR(ISD-d)*, for each scenarios.

The performance curves are given in terms of BER and throughput, for the 3 modes of Table 1. The throughput is given in percentage of the maximum achievable throughput, i.e. 100x(1-FER).

The Inter Site Distance is 500 m.

3.2.2.4.1 Mode 1

Results for mode 1 are given on Figure 8 and Figure 9. With this robust mode we can see that with no cooperation (curves with circles) the performance start degrading from a distance *d*=180 m from eNodeB1 (the throughput falls and the BER raises). With cooperation (curves with triangles) we reach the maximum performance (BER of 0 and 100 % throughput) starting from distance d=130 m.

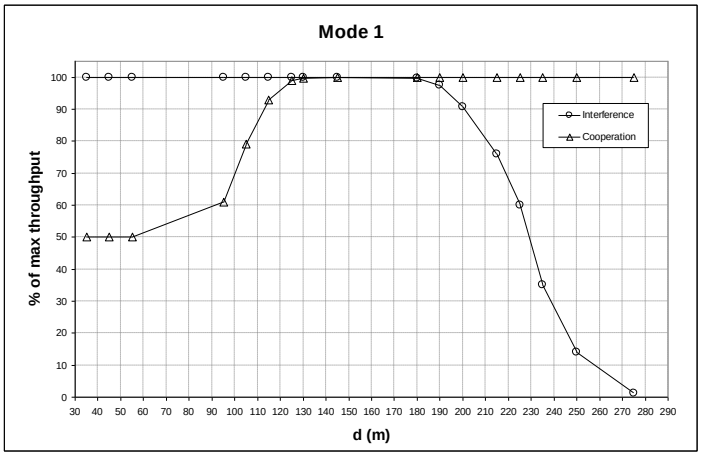

Figure 8: Throughput, mode 1

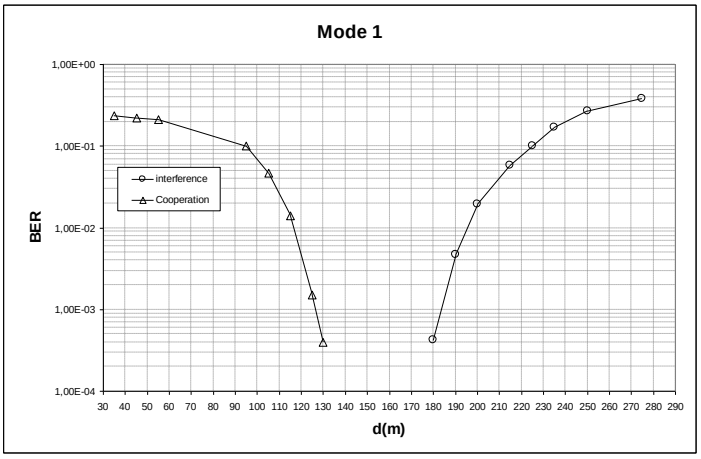

Figure 9: BER, mode 1

If we consider a UE in cell 1 for mode 1, the interference free and cooperation zones are then the one given by Figure 10. In this mode, maximum performance can then be reached wherever the UE is situated in cell 1 by choosing the appropriate interference / cooperation transmission mode as a function of the distance *d*.

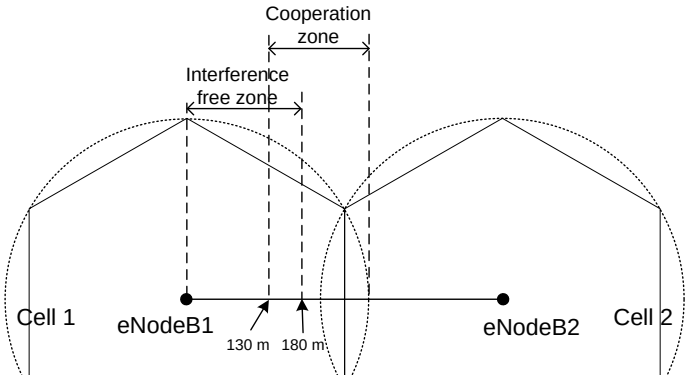

Figure 10: Interference free and cooperation zones for mode 1

3.2.2.4.2 Mode 3

Results for mode 3 are given on Figure 11 and Figure 12. In this mode, with no cooperation the performance start degrading from a distance *d*=150 m from eNodeB1, as expected smaller than the case in mode 1 as mode 3 is less robust. With cooperation we reach the maximum performance starting from distance d=175 m.

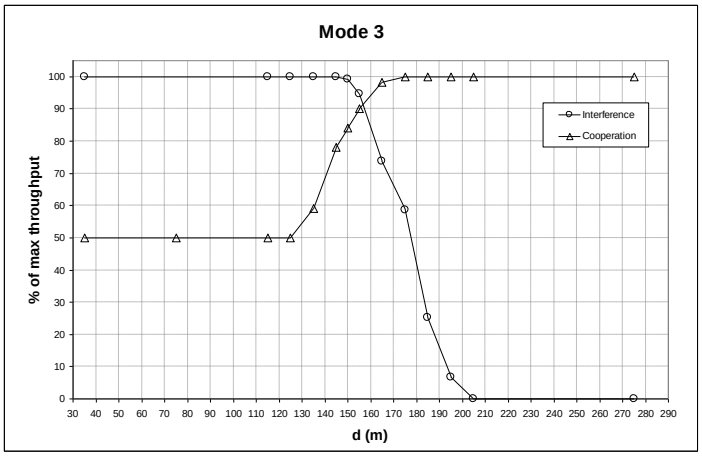

Figure 11: Throughput, mode 3

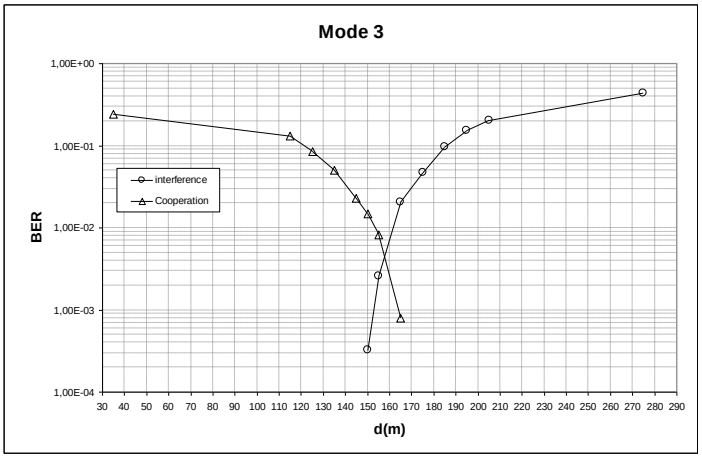

Figure 12: BER, mode 3

If we consider a UE in cell 1 for mode 3, the interference free and cooperation zones are then the one given by Figure 13. In this mode, maximum performance cannot then be reached for a UE situated at a distance *d* lying between 150 m and 175 m from eNodeB1.

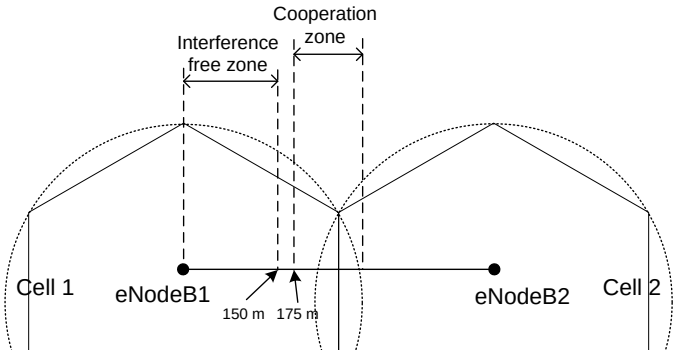

Figure 13: Interference free and cooperation zones for mode 3

3.2.2.4.3 Mode 5

Results for mode 5 are given on Figure 14 and Figure 15. In this mode, with no cooperation the performance start degrading from a distance d=130 m from eNodeB1, again smaller than the distance in mode 1 and even than that of mode 3. With cooperation we reach the maximum performance starting from distance *d*=200 m.

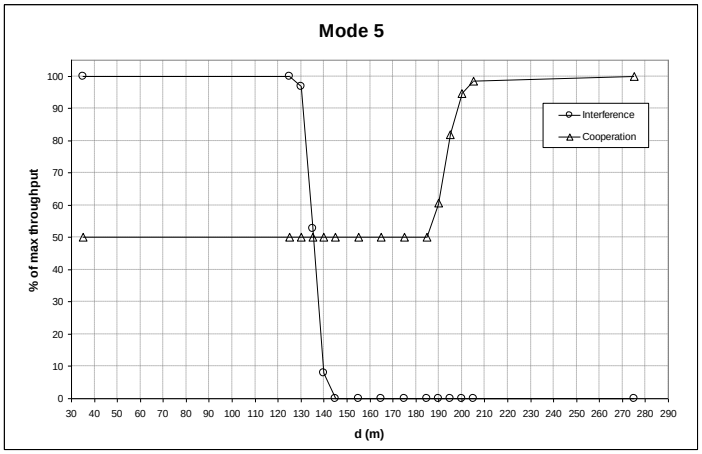

Figure 14: Throughput, mode 5

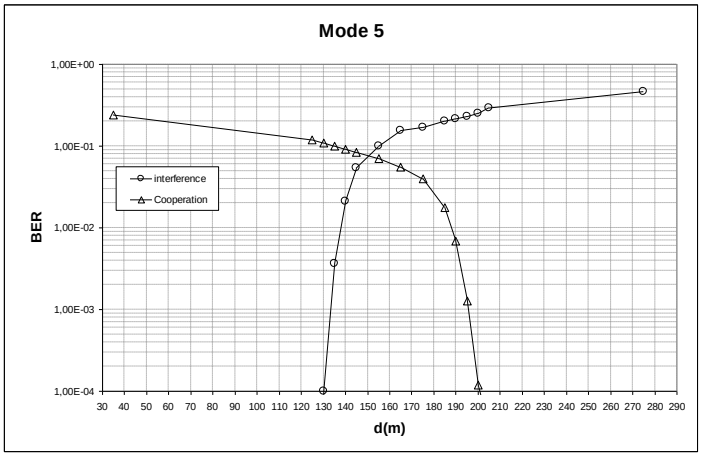

Figure 15: BER, mode 5

If we consider a UE in cell 1 for mode 5, the interference free and cooperation zones are then the one given by Figure 16. In this mode, maximum performance cannot then be reached for a UE situated at a distance d lying between 130 and 200 m from eNodeB1.

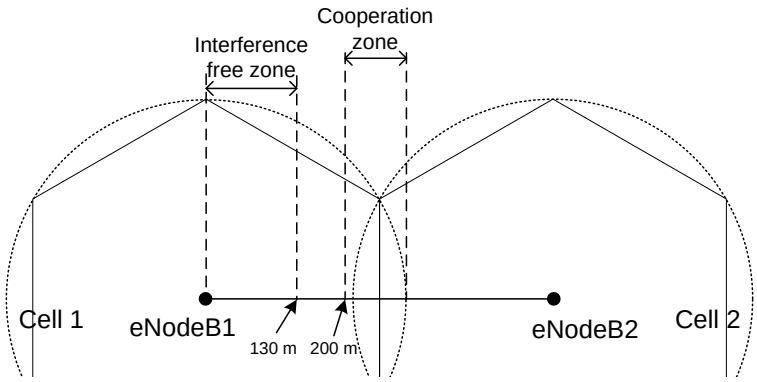

Figure 16: Interference free and cooperation zones for mode 5

3.2.2.5 Conclusion

In this study we have first shown that when no specific method (cooperation, relaying, interference mitigation…) is used, a UE near the cell edge experiences interference that dramatically damages its performance. This is especially true for a high rate mode like mode 5 with which the interference becomes too strong from a distance of only 130 m (for ISD = 500 m) from the eNodeB.

We then introduced cooperation between adjacent cells thanks to Double Alamouti decoder at the UE side. We have shown that this method allows cell edge users to reach good performance, for all of the 3 tested modes.

Nevertheless, for less robust modes, modes 3 and 5, there is a zone where the UE experiences strong interference and in the same time where the cooperating eNodeB2 is too far away to allows efficient cooperation. A solution would be to adapt the transmission mode and method to the distance of the UE from eNodeB1 in order to maximize the data rate and to minimize the BER, like proposed in Table 3.

Table 3: Adaptation of the mode to the distance

Distance from eNodeB1 (m)	Mode	Cooperation
0 to 130	5	No
130 to 150	3	No
150 to 175	1	No
175 to 200	3	Yes
200 to 280	5	Yes

3.2.3 Feedback on 2x2 Downlink Transmitter Hardware Implementation

At the time of writing, the final setup of Virtual Double Alamouti testbed was not ready. As a consequence, the simulation results provided in the previous section will be compared with lab measurements in the next deliverable of WP6. This section highlight implementation results on the second step of our implementation workflow.

3.2.3.1 Functional Description

The CEA uplink transmitter is described in Figure 17.

Upon reception of the Transport Block (TB) from the MAC layer, TB are segmented if needed into a number of equal length blocks with size equal to one of the basic TBS (Transport Block Size). A CRC is attached to each segment of the TB in order to perform error detection at the receiving side. Information bits are then scrambled with a pseudo-random sequence to avoid detrimental effect of long sequences ‘0’ or ‘1’ potentially produced by the source code. In the prototype, blocks of information bits are encoded using a duo binary Turbo Code with mother code rate equal to 1/2. The demonstrator supports three basic target code rates: 1/2, 2/3 and 3/4. The desired channel coding rate is obtained by puncturing. After channel encoding, channel interleaving is performed over the entire sub-frame to benefit from time and frequency diversity gain at the channel decoding level. The resulting bits are converted into M-ary symbols according to the modulation order (mapping). To simplify the implementation, the prototype only supports 3 MCS between the robust (QPSK, 1/2) mode to the spectrally efficient (64QAM, 3/4) mode with the intermediate (16QAM, 2/3) mode in-between.

The M-ary symbols resulting of the mapping are then fed through the MIMO encoder (Alamouti Scheme). The Base Station then performs the so-called PRB mapping that allocates to the time/frequency grid defined by a sub-frame the MIMO encoded symbols. The framing module then multiplexes reference symbols with data. It also inserts for each of OFDMA symbols the null values that modulate sub-carriers at the edges. The result of the framing is processed by the OFDM modulation module to form the sampled version of each OFDM symbol. For each antenna, this module performs an Inverse Fast Fourier Transform (IFFT) and guard interval (the cyclic prefix) insertion.

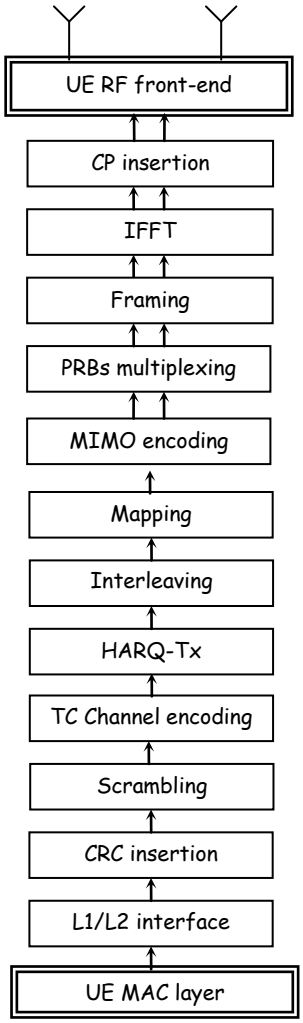

Figure 17: Functional description of the UL 2x2 transmitter

3.2.3.2 Application Mapping and Simulation Results

In this section, we will focus on how the transmission chain (TX) is mapped into the MAGALI chip and how hardware mechanisms for runtime reconfiguration are exploited. We will also provide some processing performance results extracted from our co-simulation (SYSTEMC/VHDL) environment.

3.2.3.2.1 Application mapping

For the mapping, we consider a configuration scenario corresponding to the process of one TTI which is the basic granularity for frame decoding in this application. In terms of data, a TTI represents the modulation of 14 OFDM symbols of 1024 subcarriers in a constrained time of slightly less than 1ms. For the TTI modulation, the application is split in 3 execution phases whose data flows are presented Figure 18**.**

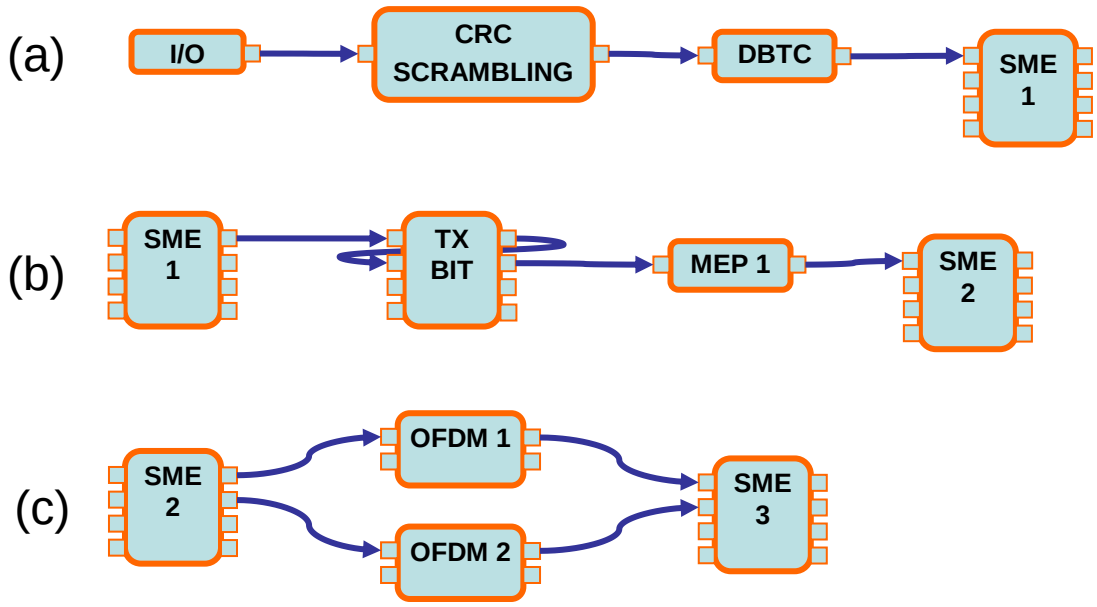

Figure 18: Application data flows after mapping

Compared to the RX application (see D6.1 [20], paragraph 3.3.1.3), the mapping of the TX application on the physical hardware resources leads to less complex data flows. Indeed, this application never reuses the same unit and algorithms are not split on different units. SME resources are also widely used for buffering intermediate results whereas, at functional level, memory aspects are not taken into accounts.

The TTI modulation scenario is divided into 3 distinctive phases, in phase (a) a CRC code is calculated and the data are scrambled. Results are encoded by the turbo encoder (DBTC). In phase (b), the SME1 has to make word interleaving before sending the data to the bit interleaver (TX BIT) and then the MEP1 (MEPHISTO DSP #1) computes the MIMO encoding. The last phase (c) is the OFDM modulation. It is computed by OFDM 1 and OFDM 2 hardware operators. The data flows on the OFDM outputs will be the inputs of each antenna and are temporary stored in SME3.

At the beginning of a TTI, resources are reconfigured by the Host CPU, to map the corresponding data flows and functions. Then, during a phase, thanks to the CCC configuration and synchronization mechanisms (see D6.1 [20], paragraph 3.3.1.2), resources are fully autonomous to execute the correct configurations for communication and processing. The full TX application never reuses the same processing unit and algorithms are mapped on distinct operators. As a consequence, only one configuration is required for each operators, and there is no need of re-configuration between the processing phases.

3.2.3.2.2 Simulation results

Results are measured on a co-simulation environment. The units are depicted in SYSTEMC-TLM or in VHDL except the ARM11 processor which is an untimed functional model.

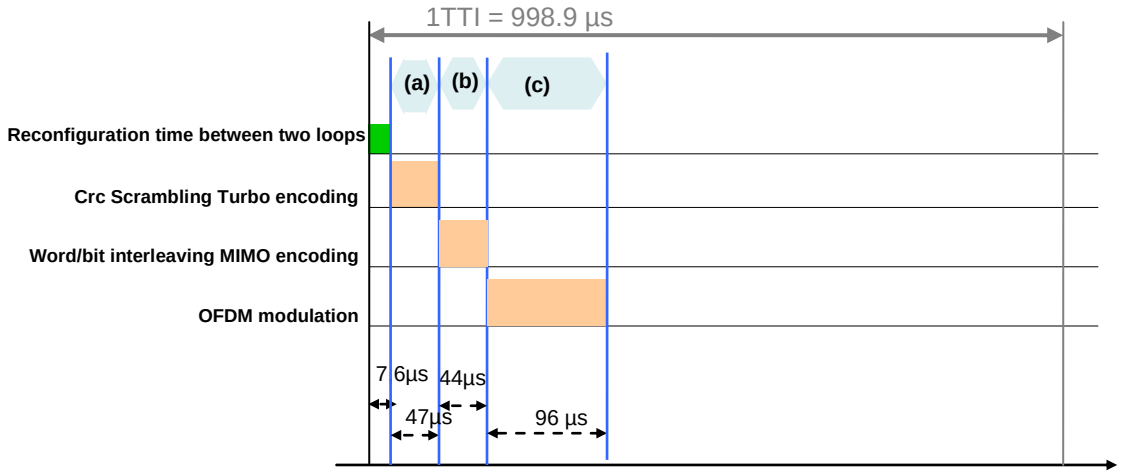

Figure 19: Application mapping chronogram

Figure 19 represents the chronogram of the TTI encoding for the worst case scenario (highest throughput) corresponding to the operating mode (5) detailed in Table 2 of D6.1 [20]. All of these phases can be pipelined without any reconfiguration in-between since they do not involve the same units and each phase is ended by a memory component (SME).

Table 4 sums up simulation results on configuration times, processing times and amount of transferred data for mode (1), (3) and (5). The whole system initialization takes 7.7µs for a whole TTI and represents less than 1% in time and in number of data packets. But this duration is a minimum value due to the untimed ARM model of our co-simulation environment. As expected, for the processing time, phases (a) and (b) are dependent on the operating mode while (c) is not.

Table 4: Reconfiguration results on 3GPP/LTE TX

	Mode 1	Mode 3	Mode 5
Re-initialization	7.677 µs		
Phase a	2.546 µs	10.46 µs	47.08 µs
Phase b	4.705 µs	9.1 µs	44.25 µs
Phase c	96µs		
TTI duration	117 µs	129 µs	192 µs
Reconfiguration flits	623		
Total sent flits	95624	96376	102896
Overhead NoC protocol	25.0%	25.1%	25.2%

Compared to the Rx chain, the number of reconfiguration flits is lower in the Tx chain, indeed the units do not need to change their configurations during a TTI and their core configurations are not reloaded if the previous TTI has the same mode. The percentage of the reconfiguration data overhead is directly linked to the high-flexibility of the platform and it can be decreased by optimizing some configurations in the network interfaces. Finally, a reasonable overhead is introduced by the NoC protocol for data routing and addressing.

3.2.3.3 Performance Measurements

3.2.3.3.1 Metrics to be measured, measurement setup and results

The Magali board includes an ARM11 processor, dedicated to the management of applications. More precisely, the ARM11 processor is intended to configure the different units of the board, to start them and to schedule the different tasks of the application. The ARM11 processor is informed that a task is executed by receiving interruptions sent by units.

For the full TTI modulation scenario, the ARM11 processor configures units involved in the processing of the 3 phases, start the computation, and wait for an interruption indicating the end of the TTI processing.
We use the ARM11 processor to monitor performance during the TTI modulation scenario, by using timers to measure the duration of each task of the ARM11 and of each operating phase.

Figure 20 represents the chronogram of the TTI processing implemented on the Magali board.

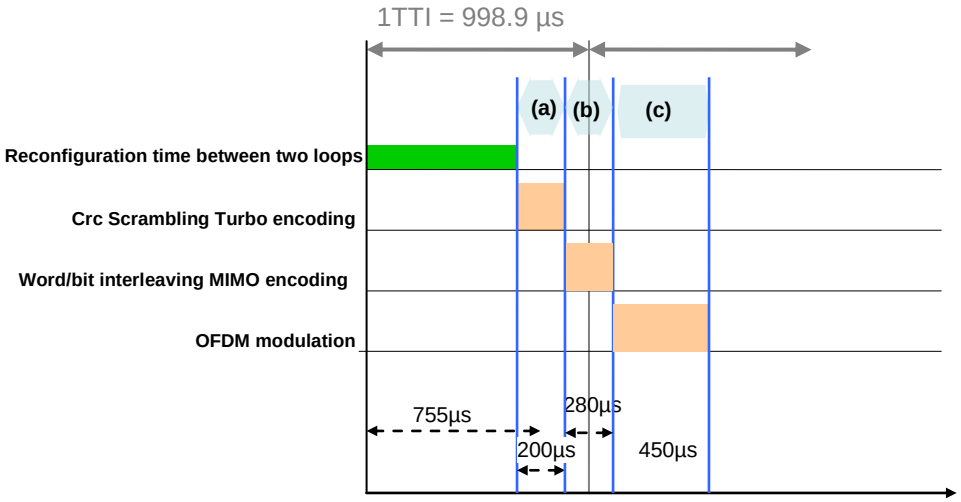

Figure 20: TTI processing chronogram on Magali board

3.2.3.3.2 Comparison with expected results and possible improvements

Compared to the simulation chronogram, one can see that the reconfiguration time is longer. The main reason is that, in the real application, we also measure the ARM11 runtime software which is not the case with the simulation results where the ARM11 model is untimed. Moreover, this runtime software has not been optimized: for example, to send one simple command with one header and two data flits, takes 10 µs. Even if the number of data to be sent with the ARM11 is quite low (a few percent of the overall 623 reconfiguration flits), the timing impact of this process is dominating the reconfiguration time. A deep optimization of the ARM11 runtime software is required for achieving results close to simulation, but this work is not the purpose of this project.

The ARM processing can be divided in two main tasks:

a. Configuration of the units (depicted in dark green). This task is computed once for the complete TTI modulation. It mainly includes a pre-processing of the configurations to be sent and the dispatch of the configurations depicting the dataflow to be processed. This task also concerns some other configurations (set of interruptions, set of some hardware registers on units, etc…).

b. Start of units and wait for interruptions. This task is done for each units involved in the processing phases. The effective processing of each phase is depicted on the line of each unit (pink areas). Time measurements being taken from the ARM11, the effective processing of each phase also includes the travel times through the NoC of the start packets from the ARM11 to the units, and of the interruptions from the units to the ARM11 (to inform it of the end of the phase). Once again, even if the involved data is quite low, the additional time of this ARM11 task makes the measured processing time longer than the simulation one.

As we have seen for the RX application, the OFDM modulation on the board does not match performances expected by simulation. This is the consequence of a problem in the OFDM modulation circumvented by a software solution: each OFDM symbol is processed sequentially (i.e., the ARM11 starts the processing of a symbol, waits for an interruption, and then treats the next symbol). This software fixing, decreasing performances because of time spent by communication between the ARM11 processor and OFDM units, could be also replaced by a hardware update which would be a more elegant solution.

In order to improve real time processing performances, further optimization could be performed on the ARM11:

a. Firstly, one could remove the time needed for pre/post processing of configurations, executing those off-line.
b. Secondly, some units have not to be reconfigured/reinitialized at each TTI if the mode has not changed, but currently all of them are reinitialized at each TTI.
c. Thirdly, some steps can be pipelined because none of the units are used twice in the Tx application.

3.3 Decentralized and Centralized Uplink CoMP Schemes

3.3.1 Introduction

The spectral efficiency of today's cellular systems is limited by inter-cell interference. Especially data rates for mobile users that are located at cell edges are strongly reduced by this effect, resulting in a lack of fairness that is identified as one of the major deficiencies of LTE Release 8. The major objective of the research done in ARTIST4G is to propose and investigate methods reducing this effect. Some of the most promising proposals that are being discussed in ARTIST4G WP1 and WP2 for an improved system setup consider using CoMP techniques for the up- and downlink. A concise overview on this topic is given in [19]. Theoretical analysis and simulations promise significant increases in spectral efficiency, e.g. [3]. However, an important question is if today's technology is ready to support such ambitious concepts. In part, this question was already answered in the EASY-C project. Field trials of a setup of up to 12 base stations were reported in [4-6]. For the cellular uplink, it has been shown that joint detection in the cellular uplink increases the spectral efficiency by about 50 % for a setup with single antenna BS and limited cooperation cluster size of up to three BSs. Additionally, the rate distribution over the measurement area was smoothed out, showing that fairness is improved strongly by using cooperation.

The focus of the work done in ARTIST4G was on the extension of these field trials. In particular, we concentrated on

- more flexible system setups with up to two antennas per BS.
- the investigation of backhaul constraints for joint detection (JD).
- the impact of the downtilt on system performance.

3.3.2 Measurement Setup

For a detailed description of the basic measurement setup and concept that is used in all field trials reported in the following we refer the reader to [7]. The testbed that was used is shown in Figure 21. It consists of a 16 BSs that are located at seven sites in the downtown of Dresden. The UEs are carried on a measurement bus or on bicycle rickshaws. In all field trials that are presented in this deliverable, we use up to two UEs, but in the course of the project it is planned to increase this number further.

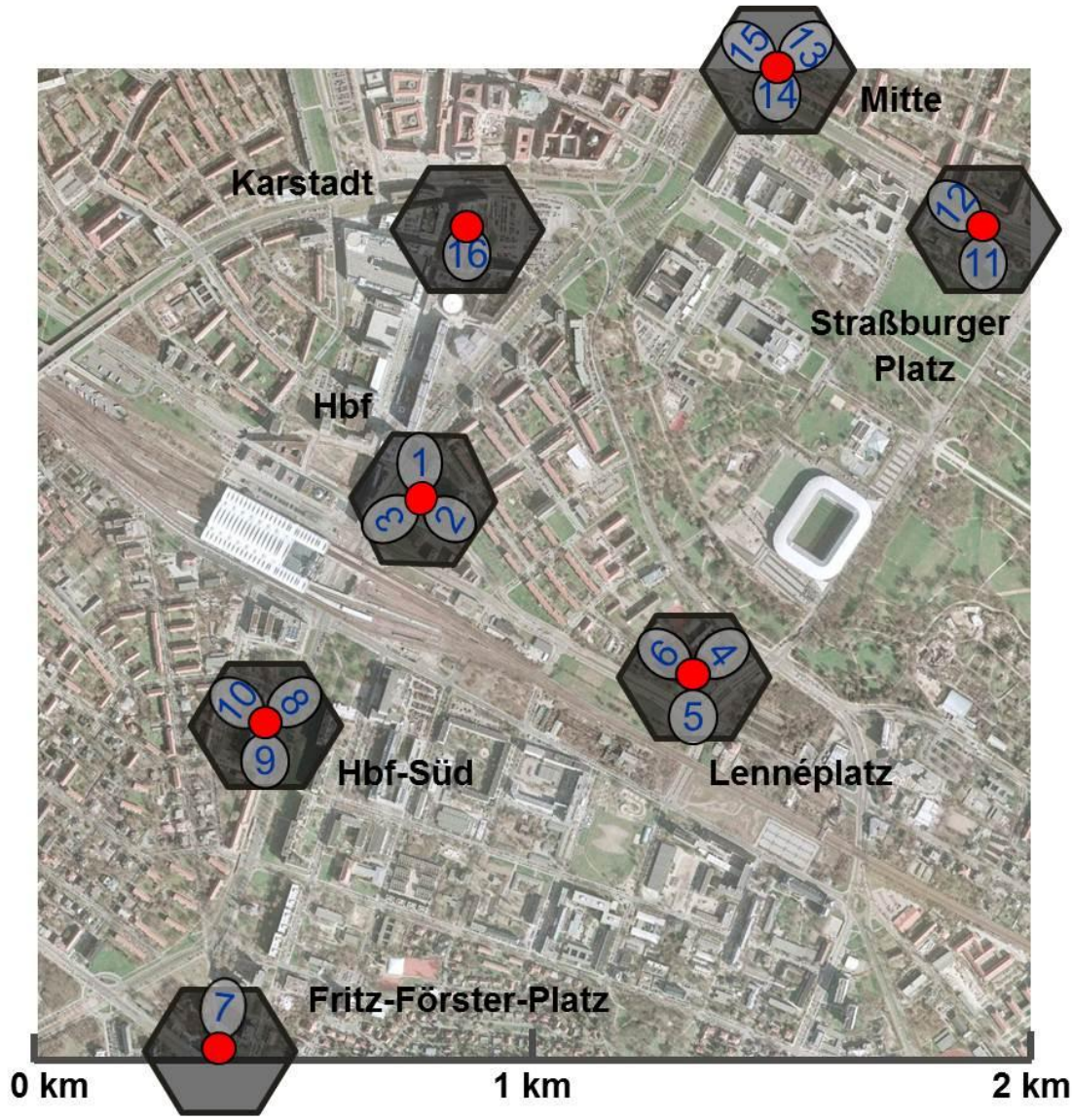

Figure 21 Field trial setup and BS locations of 16 BSs in downtown Dresden. Map data © Sandstein Neue Medien GmbH (http://stadtplan.dresden.de)

3.3.3 Signal Processing Architecture

The signal processing architecture is described in [7], in detail as well. All BS signal processing is done offline, allowing flexible testing of different receiver and cooperation algorithms. The drawback of this approach is that a real-time feedback from the BSs to the UEs is not possible as it would be required for rate adaptation and scheduling.

3.3.4 Results

In the following three sub-sections, we will present results of the uplink CoMP field trial activities of the first 18 month of ARTIST4G. Results that are already published in specific conference papers are only summarized briefly. For further information we will refer to those papers.

3.3.4.1 Large Scale Field Trial on Multi-Antenna Base Stations

Previous field trials for uplink CoMP that were done in EASY-C have shown that large improvements in spectral efficiency and fairness that are promised by theoretical work can also be achieved in real-world scenarios [6]. However, these results only consider systems with single antenna base stations. In ARTIST4G, we have extended this work by presenting field trial results for a system with multi antenna base stations. The change of the system setup has a strong impact not only on the throughput but also on the relative performance of a cooperative compared to a non-cooperative system. Since the results of this work are presented in [8], we only give a short summary at this point. In the large-scale field trials, the performance difference

between non-cooperative and cooperative uplink detection schemes was investigated. The considered cooperation schemes are joint detection (JD) and distributed successive interference subtraction (DSIC). In addition, we compared the performance of linear detection and successive interference cancellation (SIC). Two UEs were moved through an urban cellular test bed with a total of sixteen BS. For the evaluation of results, either one or two antennas per BS were considered. Observing the one-antenna case allows the prediction of gains in setups with two UE per cell served on the same resource, or UE with two transmit antennas each. Compared to non-cooperative linear detection, local SIC already increases average spectral efficiency by about $19\,\%$ or $7\,\%$, for the different antenna setups, respectively. On top of this, multi-cell joint detection yields an average gain of $52\,\%$ or $15\,\%$, for one or two BS antennas, respectively. As expected, particularly strong gains are visible at cell-edges, which can in some cases already be achieved through intra-site CoMP.

3.3.4.2 Time Domain Compression

The results of the field trial evaluation that were presented in the previous section confirm that JD achieves better performance than distributed cooperation schemes such as DSIC, as it was already predicted by earlier information theoretic studies (e.g. [3]). On the downside, JD requires a vast amount of data traffic to be exchanged over the backhaul. However, recent studies promise great performance of JD even under stringent backhaul constraints provided that the exchanged signals are compressed. A first field trial performance and complexity study of different compression schemes was published in [9]. However, here we only investigated a small setup with 2 BSs and 2 UEs. In a next step, we investigated the limits and potentials of this approach in a practical setting using the same field trial data as in the evaluation above,

In particular, we compared conventional non-cooperative detection to cooperative JD, where the backhaul requirements were reduced by using compression of the exchanged time domain signal. The average sum-rate could be increased linearly with the compression rate until a threshold of about 4 bit per real symbol which corresponds to a backhaul rate of about 288 Mbps for the field trial setup investigated. For a detailed description and evaluation of the results, we refer the reader to [10].

3.3.4.3 Impact of Downtilt

The field trial results presented above verify large improvements in spectral efficiency and fairness that were previously predicted by theory and simulation studies. In practical systems, however, the number of BS that can cooperate for the detection of a certain set of UEs is limited because of the required pilot signal overhead, as well as backhaul and latency constraints [3]. The particular set of BS that cooperate to detect a certain number of users is referred to as a cooperation cluster. The vast number of interferers outside the cluster add to an interference floor that limits the achievable signal-to-outer-cell-interference ratio (SOCIR) and, therefore, the system performance. Thus, cooperation of BS needs to be applied jointly with other methods for inter cell interference reduction. An outstanding lever, that is successfully exploited in the roll out of previous cellular standards, is to adapt the antenna radiation pattern with the aim to reduce inter-cell interference by taking the deployment and physical layer characteristics into account. For this purpose modern BS antennas typically provide mechanical and electrical means for a modification of their downtilt (the elevation angle corresponding to the highest directional antenna gain). The impact of the downtilt on system performance is well studied for WCDMA [11], but possible cooperation of BS certainly has an impact on optimal downtilt settings as addressed and investigated by simulations in [12]. In this section, we investigate the impact of antenna downtilt on a CoMP uplink in a large scale field trial where two UE are detected at clusters of up to three BS. For this setting, we show that while achievable rates are only marginally effected by the downtilt, outer cluster interference can be substantially reduced by increasing the antenna downtilt, i.e. reducing the distance where the main antenna beam first hits the ground.

As in the field trial of the previous section, general setup consists of 16 BS deployed at 7 sites in downtown Dresden, as shown in Figure 1, and two UE that are assembled on a measurement bus. Each BS is equipped with a two element, cross-polarized KATHREIN 80010541 antenna which has 58° horizontal and 6.1° vertical half power beam width. We refer the reader to [12] for an illustration of the radiation pattern of this antenna. In order to investigate the impact of the BS antenna downtilt the measurement route is repeated for four different downtilts between 0° - 12°

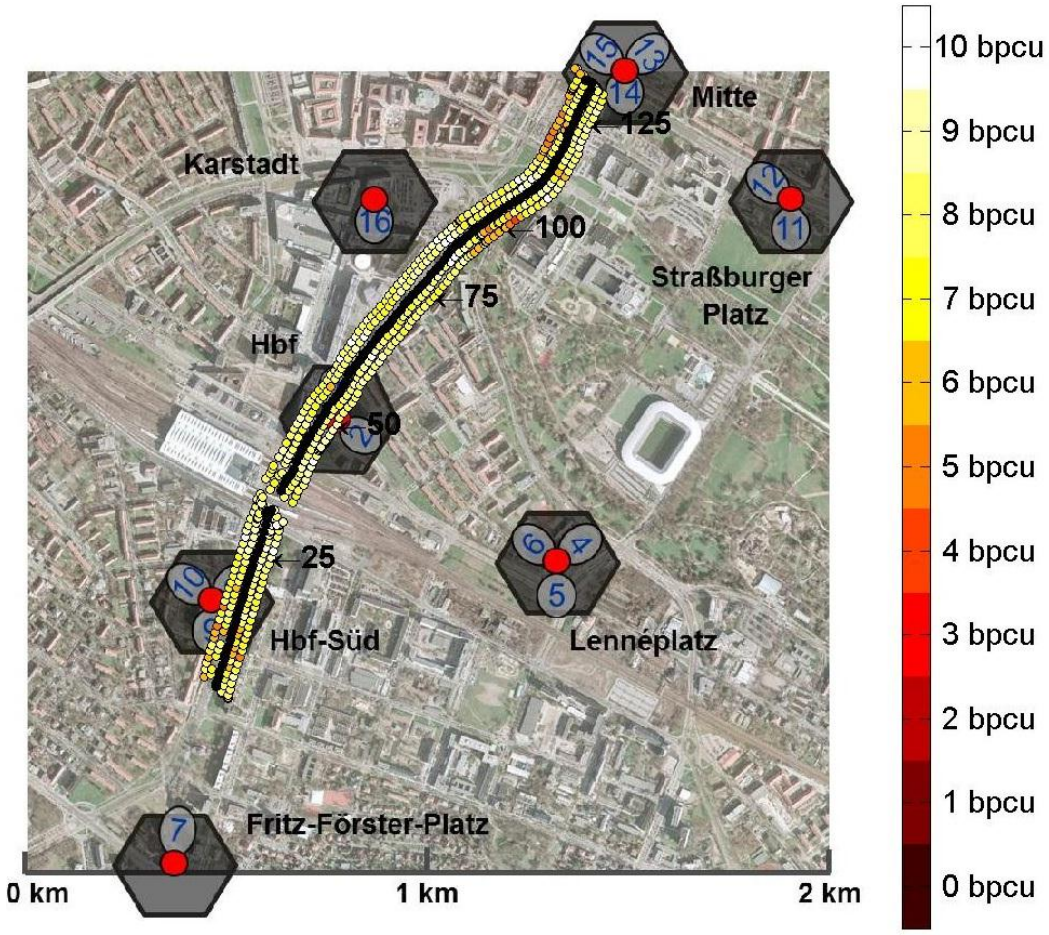

Figure 22 Field trial setup and measurement trajectory (black curve). The other curves indicate the sum rate achieved by joint detection of 2 UE at two cooperating BS with $N_{bs} = 2$ antennas each. Each curve is showing the result for a particular antenna downtilt (at each BS of $\Phi_t = 0^\circ, 6^\circ, 9^\circ, 12^\circ$ from the left to the right. Map data © Sandstein Neue Medien GmbH (http://stadtplan.dresden.de)

The route traversed by the measurement car, traveling at a speed of about 6 km/h, is depicted in Figure 22 (black curve). It passes through surroundings that are representative of an urban area, characterized by broad roads with two lanes in each direction as well as tracks for trams, and sidewalks on either side. Both sides of the road are flanked by large apartments of more than 20 m in height. Thus, there is often a LOS between the UE and one or more BS.

During the field trial, the BS captures an 80 ms block of their received signal every 10 s. At the same time, UE continuously transmits codewords (each spanning 1 TTI (1 ms)) continuously, switching cyclically through all 8 MCS given in Table 2 --- ranging from low code rate 4QAM to high code rate 64QAM. For each loop through all MCS, the maximum achievable rate is determined --- assuming a constant channel for at least the duration of one loop --- by emulating a perfect rate adaptation. The achieved rate is obtained by averaging over all loops of one measurement and denoted by $r_{k,p}$ for UE k and position p. For further information on field trial evaluation procedure we refer the reader to [6]. The BS that are considered for joint decoding of the UE are determined by a minimum pathloss criterion while UE, in the non-cooperative case, are decoded at the BS that is able to decode the highest rate codeword.

Table 5 Modulation schemes and code rates used for transmission.

MCS#	Mod. scheme	Code rate	Peak rate (Mbps)	Bit per channel use (bpcu)
1	4QAM	3/16	1.3	0.375
2	4QAM	1/2	3.46	1.0

3	16QAM	2/5	5.62	1.6
4	16QAM	4/7	7.99	2.29
5	16QAM	3/4	10.6	3.0
6	16QAM	6/7	12.3	3.43
7	64QAM	3/4	16.3	4.5
8	64QAM	7/8	18.72	5.25

In summary, the field trial is subject to the following assumptions and limitations:

- Assignment of the same resources to UE located with fixed distance in close proximity is rather unlikely in a non-cooperative cellular system with single antenna BS.
- No rate adaptation and HARQ due to offline signal processing. The genie rate adaptation scheme (described above) diminishes the diversity gain of JD because each codeword can be decoded at a different BS even in the non-cooperative case.
- No background interference has been considered and, thus, no interference floor is visible.
- Both UE transmit continuously at maximum power.

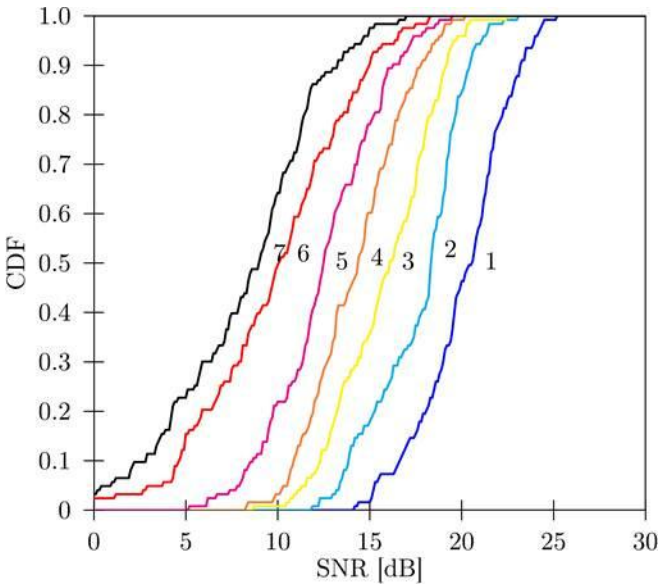

a) $\Phi_t = 0^\circ$

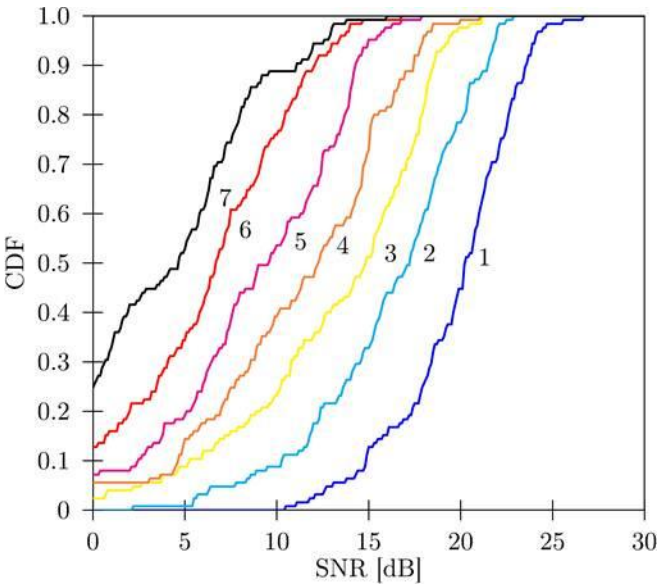

b) $\Phi_t = 6^\circ$

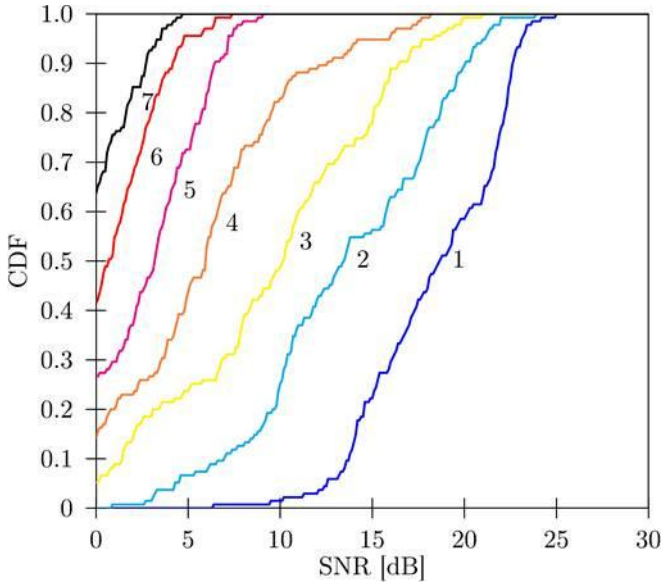

c) $\Phi_t = 12^\circ$

Figure 23 CDF of SNR instantaneously achieved at a certain number of BSs.

In order to study the impact of the BS antenna downtilt, the same route was traversed for different downtilts of $\Phi_t = 0^\circ, 6^\circ, 9^\circ, 12^\circ$. Figure 22 shows the sum rate ($r_p = r_{1,p} + r_{2,p}$) that was achieved for JD of two BS with $N_{bs} = 2$ BS antennas at each measurement point for each downtilt considered. We see that the sum rate shows rather little fluctuations which is a benefit of JD as shown in a previous publication [6]. Please note that the measurements with different downtilts were conducted one after another. Thus, certain variations in the surroundings and measurement locations were inevitable. However, we will focus on a statistical evaluation in the following for which the accuracy of the results was tested by additional calibration measurements.

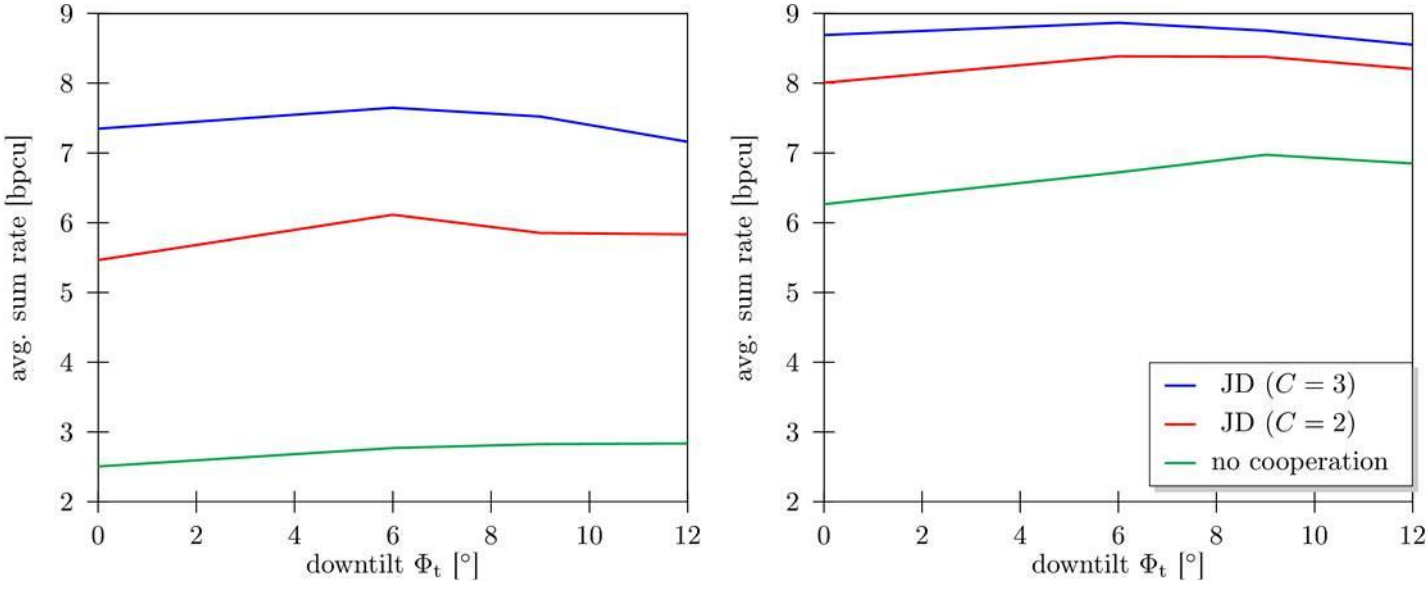

$N_{bs} = 1$ $N_{bs} = 2$

Figure 24 *Avg. rate over downtilt for either one or two BS antennas*

Figure 23 shows the CDF of the SNR that is achieved simultaneously at an increasing numbers of BS for different downtilts of $0, 6, 12^\circ$. Comparing the case of $\Phi_t = 0^\circ$ with the case of

$\Phi_t = 6^\circ$, we see that the variance of SNR increases with downtilt because the reception of signals at larger tilts is more focused and, thereby, shows a stronger dependence on the UE location. The results also indicates the potential benefit of JD --- using two BS or more --- because a high SNR is instantly achieved at several BS. Taking the result for a downtilt of 6° as an example, we see that the SNR at three different BS is above 15 dB in about 50 % of the measurements. This observation is supported by the average sum-rate shown in Figure 24 for JD and non-cooperative detection. The average sum rate for a setup with one receive antenna per BS is shown in Figure 24 on the left and the case for two receive antennas in Figure 24 on the right. In both cases, the downtilt has no significant impact which is remarkable as Figure 23 shows that the average power of the received signal decreases with the downtilt. The major reason for this finding is that the UE rates are mostly limited by inter-user interference rather than by noise. In the non-cooperative $N_{bs} = 1$ case, because of an improved UE separation: the probability that both UE are decoded at the same BS is decreases steadily with downtilt from 13 % to 6 %. In the case of $N_{bs} = 2$ receive antennas per BS, the UE signals can be spatially separated at a single BS. As a consequence, detection of both UE at the same BS achieves much better results.

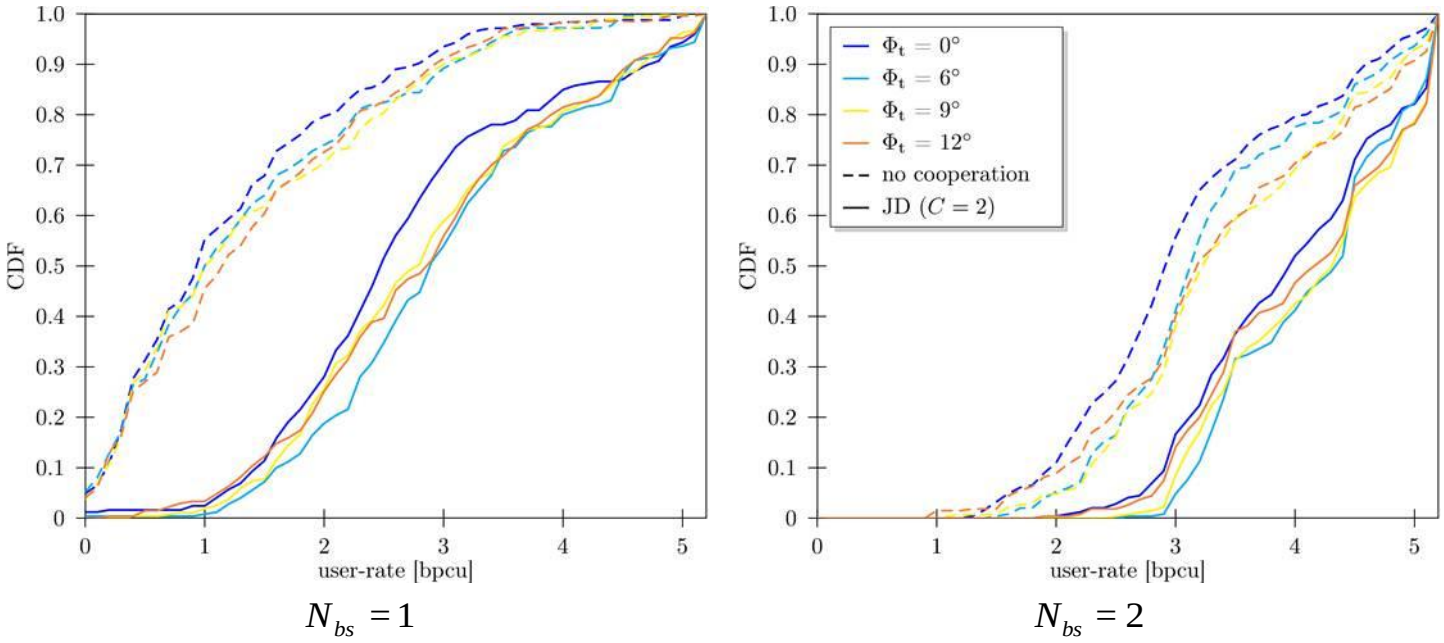

Figure 25 CDF of user rates for non-cooperative and JD of BSs

The user rate CDF for non-cooperative detection and JD at two BS are plotted in Figure 25. The curves attest the rate improvements that are achievable using JD and show that cooperation increases fairness and reduces outage probability. The curves also confirm that downtilt has only a minor impact on the user rate in our field trial system where only intra-cluster interference is considered due to limited number of UE. For cellular systems, however, outer cluster interference is an important factor, in particular because the size of cooperation clusters is limited due to practical signaling and backhaul constraints. Going back to Figure 23, we see substantial signal propagation to BS that are outside the interference cluster, where it causes interference. When we compare Figure 2a and Figure 2c, we see that the severity of this interference strongly depends on the downtilt that is applied. In case of 12° downtilt, three BS have a received signal power of about 10 dB (instead of 15 dB for $\Phi_t = 6^\circ$) in 50 % of the measurements, but, at the same time, the interference caused at other BS is substantially reduced. In order to evaluate the trade-offs we compute the SOCIR at each measurement position s which we define as

$$SOCIR(s) = \frac{\sum_{m \in \mathcal{C}} p_{s,m}}{\sum_{\forall m \setminus m \in \mathcal{C}} p_{s,m}}.$$

where $p_{s,m}$ is the total received power at BS m, for UE position (measurement) s. Thus, SOCIR is ratio of the received power inside the cooperation $\mathcal{C}$ to the received power at all BSs outside the cooperation cluster. The average SOCIR for reception at a single BS and cluster sizes of $C = 2$ and $C = 3$ is plotted in Figure 26. In the case of a single BS in the cluster, the received signal at all but one BS is considered as interference. For all cases, the average SOCIR increases with the downtilt showing that the benefit of a potentially larger average signal power for small downtilts is outweighed by the interference caused at BSs outside the cluster and thus downtilt optimization retains its important role in the deployment of cellular systems even when (partial) cooperation between BS is used.

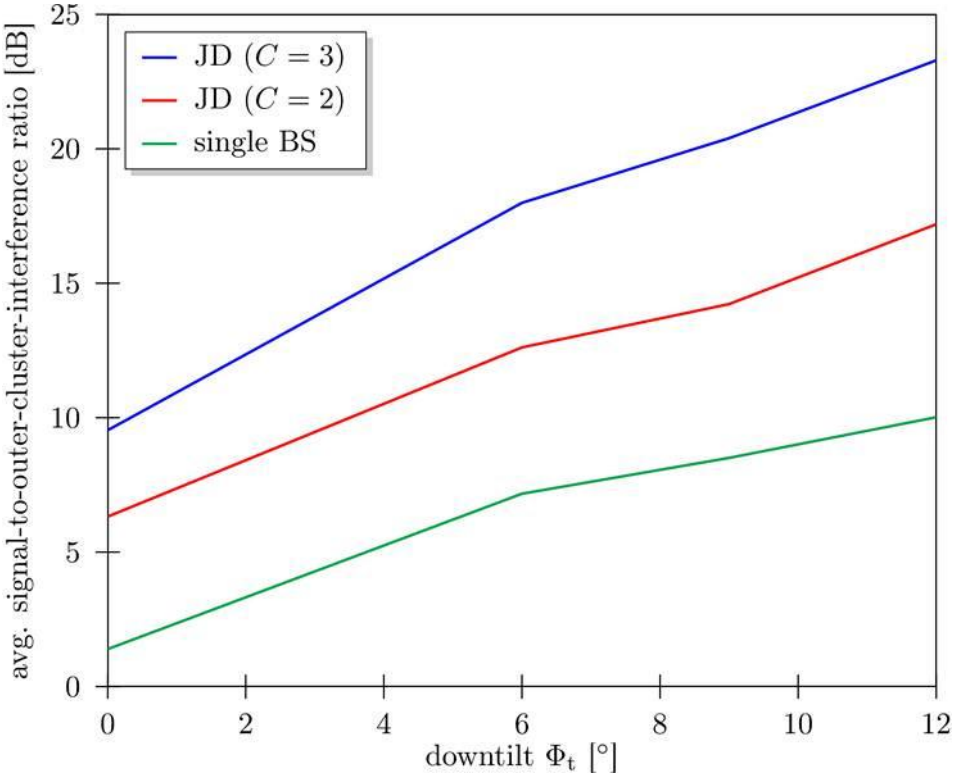

Figure 26 Average SOCIR using JD of either 2 or 3 BSs

3.4 Test of Channel Estimation Algorithms

3.4.1 Introduction

In WP2, different channel estimation algorithms have been investigated including both non-iterative and iterative ones. Complementary to the investigation of such methods in WP2, it is interesting to consider the implementation aspects of channel estimation algorithms in real systems and to investigate corresponding performances. In practical implementations, one of the key objectives is to achieve a minimum loss compared to the theory. Unless the optimizations are done properly, one may not achieve the desired performance and, depending on the implementation, the loss may lead to serious performance degradation, especially in small-scale implementations. In this manner, it is crucial to gather the results both from simulation and testbed which reflect the loss we are facing in the implementation. Moreover, having the ability to compare different algorithms in a testbed allows assessing their capabilities also in real implementation (see [20] for more detailed discussions).

Using the Sequans UE platform, we have assessed the performances of the channel estimation algorithms selected from the ones investigated in WP2 (see [13] for more details) in a real time small-scale implementation. In these assessments, our aim is to gather the results from the testbed and compare with the ones obtained from the full LTE Rel. 8/9 compliant link-level simulator. In the sequel, we first describe the test cases to be used for the lab trials together with the configurations used in the simulations. Then, we will present the results of two different channel estimation algorithms, namely, frequency-first and time-first methods which have been already discussed in detail in [13] and [20]. In particular, theoretical details and floating point performances have been already presented in [13] and implementation aspects and computational complexity analysis have been provided in [20].

3.4.2 Description of the test cases

Measurements have been carried out using the lab test setup presented in D6.1 [20]. The initial step of measurements was the sensitivity test. This corresponds to measuring the lowest RSSI which corresponds to 95% of the throughput. All done based on QPSK with the coding rate of 1/3. It has been shown that the prototype satisfies the minimum requirements from the 3GPP LTE test requirement document TS 36.101 [14] and no undesired effect has been observed in the SNR range of interest. Next, the performances of the channel estimation algorithms have been assessed from the measurement setup. The measurements have been performed for single-input (single-antenna port option as specified in 3GPP LTE specification TS 36.211) multiple-output transmission case where the receiver has 2 antennas. The simulation scenarios have been chosen mainly based on the 3GPP LTE test requirement document TS 36.101 [14] which indicates precisely the complete parameter set including the duplexing mode (TDD/FDD), DL/UL configuration, frame/subframe configurations, cyclic prefix format; control information formats and channel models (e.g., AWGN, Extended Pedestrian A (EPA), Extended Vehicular A (EVA) and Extended Typical Urban (ETU) [22]) together with the Doppler frequencies. A subset of such common simulations parameters used in the measurements is provided in Table 1. In order to test the performance of the selected channel estimation algorithms, test scenarios are defined as in Table 2 based on TS 36.101 [14].

Table 1 Part of common simulation parameters used in all test cases [14].

Parameter	Value
Uplink downlink configuration	1 (TDD)
Special subframe configuration	4
Cyclic prefix	Normal
Cell ID	0
Inter-TTI Distance	1
Number of OFDM symbols for PDCCH	2

Table 2 Scenarios selected for measurements (aligned with TS 36.101/36.133).

Test Cases	Bandwith	MCS	Channel Model
0	10 MHz	QPSK 1/3	AWGN
1	10 MHz	QPSK 1/3	EVA5
2	10 MHz	QPSK 1/3	ETU70
15	10 MHz	64QAM 3/4	EVA5

Test Case 0 is included to see the performance difference without any channel fading. The rest of the tests are realized over fading channel models EVA and ETU with 5 and 70 Hz Doppler frequencies, respectively. Table 1 provides the common configuration of all these test cases. On the other hand, depending on the MCS, the allocation of the code blocks and the payload change, which is detailed in Table 3.

Table 3 Details of DL subframe allocation for Test Cases 0, 1, 2, and 15.

	Test Cases 0, 1, 2	Test Case 15
Allocated subframes per Radio Frame (Downlink SF+Special SF)	4+2	4+2
Information Bit Payload		
For Sub-Frames 4,9	4392	30576
For Sub-Frames 1,6	3240	23688
For Sub-Frame 5	n/a	n/a
For Sub-Frame 0	4392	30576
Number of Code Blocks per Sub-Frame		
For Sub-Frames 4,9	1	5
For Sub-Frames 1,6	1	4
For Sub-Frame 5	n/a	n/a
For Sub-Frame 0	1	5
Binary Channel Bits Per Sub-Frame		
For Sub-Frames 4,9	13800	41400
For Sub-Frames 1,6	11256	33768
For Sub-Frame 5	n/a	n/a
For Sub-Frame 0	13104	39312

3.4.3 Comparison of proposed algorithms

In the sequel, we present the performance comparison of the frequency-first and time-first channel estimation algorithms which has been developed based on the analysis of D2.2 [13]. As explained in D6.1, this general comparison consists of results from

- floating point simulator (i.e. the performance assessments obtained in WP2 from the floating point simulator which provides the performance with perfect channel information),
- fixed point simulator (this simulator has been prepared in the context of WP6 and is close to the platform implementation)
- testbed implementation.

From all the tests, we have seen that the degradation between floating and fixed point is negligible for all the mentioned algorithms. Therefore, for the sake of clarity, we will focus on the fixed point and testbed results.

The performance results are compared in terms of packet error rate (PER) vs signal-to-noise ratio (SNR) curves. Here, the SNR of interest is the ratio of the average signal power per receive antenna to the average noise power.

In Figure 27, we show the performance comparison for test case 0 (AWGN with MCS of QPSK 1/3) where the PER vs. SNR curves of frequency-first channel estimation and time-first channel estimation methods are presented. Here, we can see that the results from the testbed are very close to the fixed point ones for all the methods. As expected from the floating results provided in D2.2, time-first method outperforms frequency-first. But even time-first is still far from the best achievable performance which is depicted with the perfect CSI curve. Figure 28 and Figure 29 show the performance comparison using the same frame configuration as that of Figure 27 but under fading channel conditions. In both figures, time-first method outperforms frequency-first. However, the gap between perfect CSI and these methods is quite remarkable. Specifically, the degradation goes beyond 4 dB with frequency-first method. We have at least 1 dB improvement with time-first approach for each case below PER of 10^{-3}.

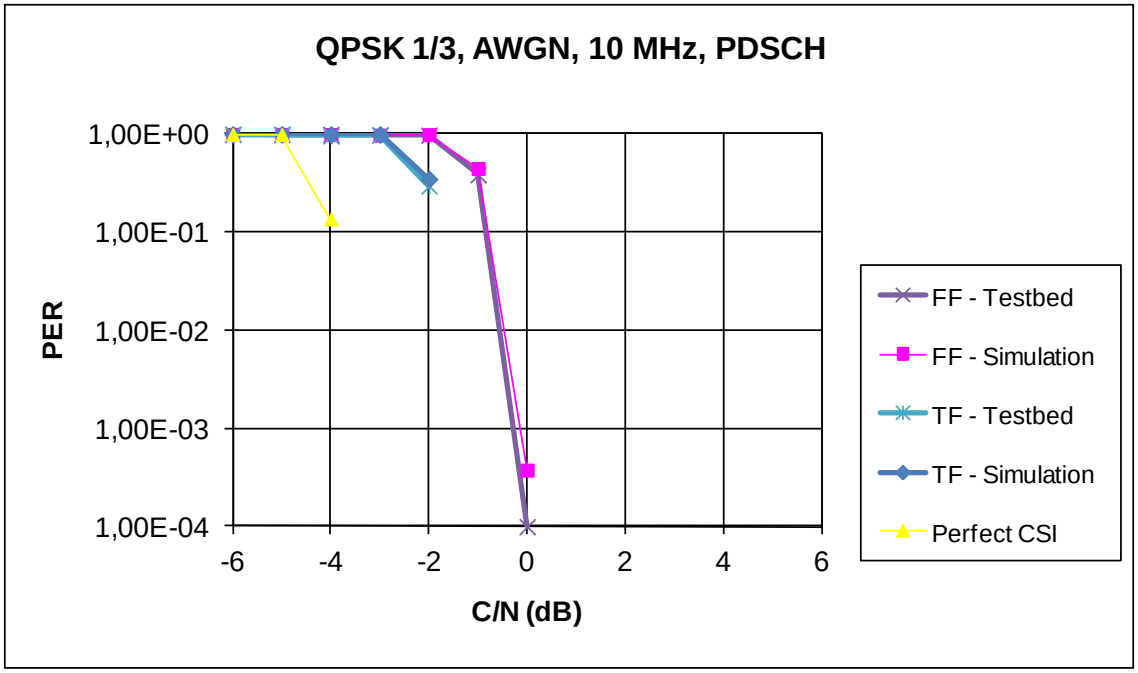

Figure 27 Performance comparison of channel estimation methods from simulations and lab testbed, test case 0.

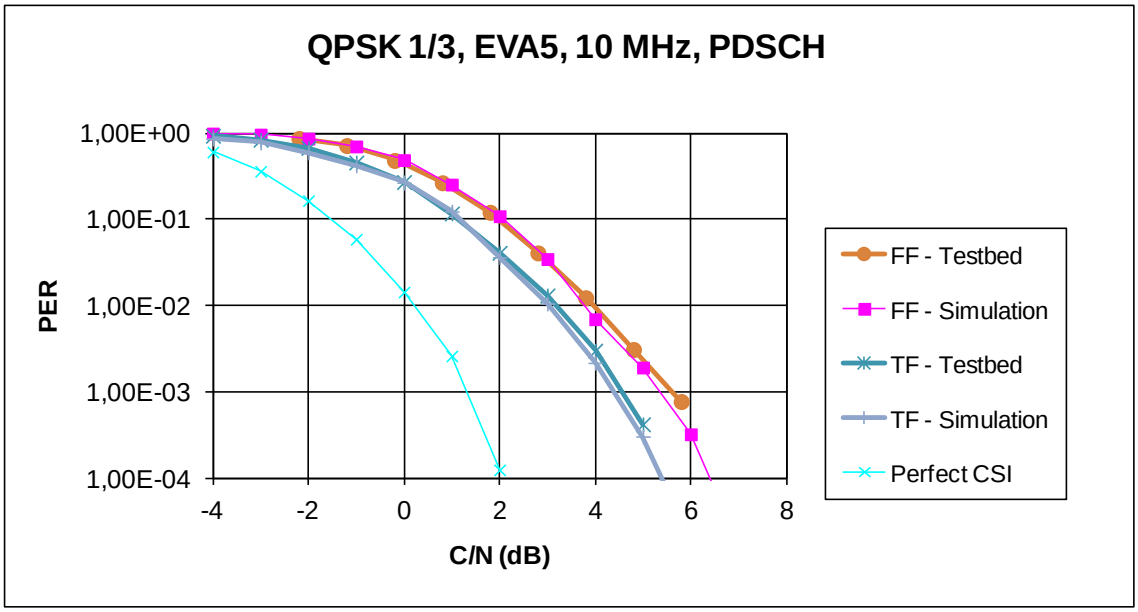

Figure 28 Performance comparison of channel estimation methods from simulations and lab testbed, test case 1.

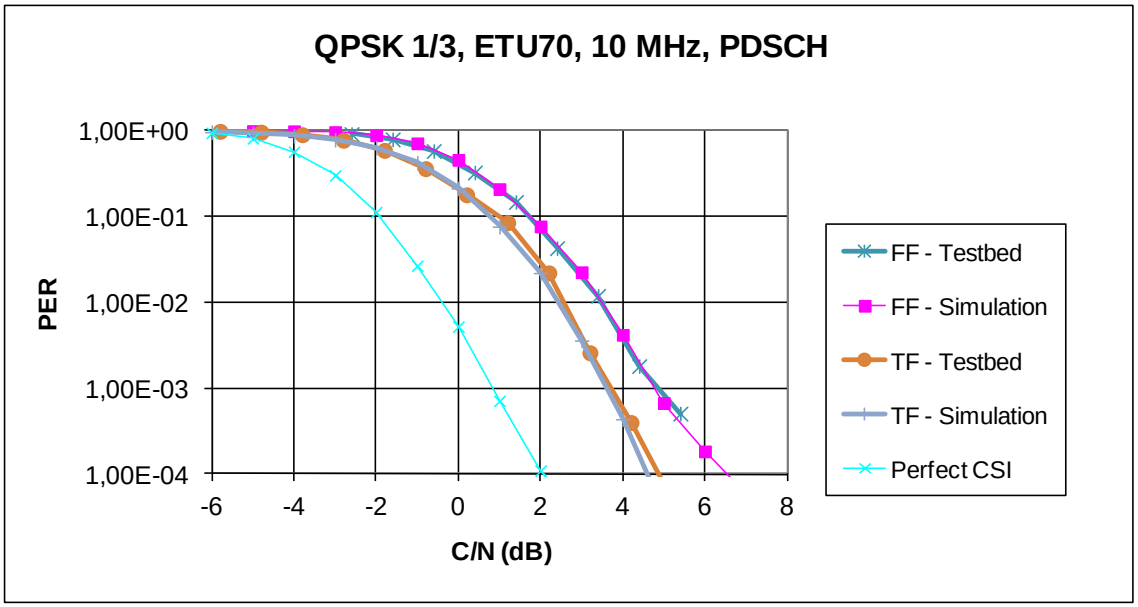

Figure 29 Performance comparison of channel estimation methods from simulations and lab testbed, test case 2.

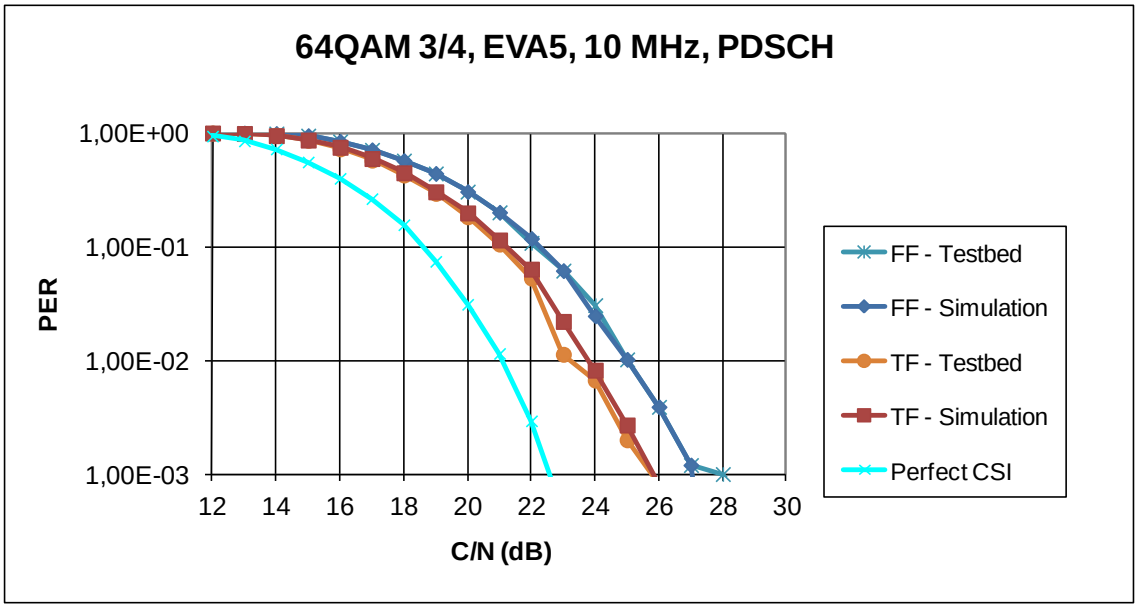

Figure 30 Performance comparison of channel estimation methods from simulations and lab testbed, test case 15.

3.4.4 Discussion

In this section, we have seen performance comparison of two different approaches (frequency-first and time-first methods) which were direct contributions from WP2 and have been already discussed in detail in [13] and [20]. Comparison results have been presented in terms of PER vs SNR performance curves in different scenarios. In all the tests, we have shown a very good matching between the simulation results and testbed results which proves the efficiency of the implementation in the platform. We have also provided some insights related to the performance differences of the algorithms. As discussed in [20], the additional complexity we introduce with time-first is really small while the performance improvement is remarkable. This makes time-first more attractive in terms of implementation. It is also worth noting that for both methods the same filter coefficients used for the sake of fairness. The performance can be improved in both cases with optimized filters.

4 Conclusions

In the deliverable, a first lab and field trial results of ARTIST4G innovations were presented. The tested innovations range from 3D beamforming to uplink and downlink CoMP and the implementation of advanced channel estimation algorithms.

A proof of concept of 3D beamforming shows SNR gains of a location dependent downtilt of about 10dB without considering interference. This is the baseline comparison with simulation results and the basis for the investigation of more complex test setups.

Feedback on the implementation of a downlink CoMP testbed using Magali boards shows the great potentials of the system on chip architecture. Simulation results of a downlink CoMP scheme, that is based on Alamouti codes and thus does not require channel feedback, are provided as a benchmark for future lab trials.

Uplink CoMP is investigated in several large scale field trials that show the great potentials of this technology. The field trials also consider compression for reduced backhaul requirements, multi-antenna base stations and the impact of downtilt.

The implementation of advanced channel estimation algorithms on the Sequans UE platform is proven to be in line with the predictions from simulations.

References

[1] "D1.2 Innovative advanced signal processing algorithms for interference avoidance," *ARTIST 4G technical document to appear*, 2010.

[2] "D2.2 - Advanced Receiver Signal Processing Techniques: Evaluation and Characterization," *ARTIST 4G technical document*, 2010.

[3] P. Marsch and G. Fettweis, "Uplink CoMP under a Constrained Backhaul and Imperfect Channel Knowledge," *IEEE Transactions on Wireless Communications*, 2011.

[4] M. Grieger, P. Marsch, Z. Rong, and G. Fettweis, "Field Trial Results for a Coordinated {Multi-Point} {(CoMP)} Uplink in Cellular Systems," *International ITG Workshop on Smart Antennas 2010*, Bremen, Germany: 2010, pp. 93-98.

[5] P. Marsch, M. Grieger, and G. Fettweis, "Field Trial Results on Different Uplink Coordinated {Multi-Point} {(CoMP)} Concepts in Cellular Systems," *IEEE Globecom*, Miami, USA: 2010.

[6] P. Marsch, M. Grieger, and G. Fettweis, "Large Scale Field Trial Results on Different Uplink Coordinated Multi-Point (CoMP) Concepts in an Urban Environment," *IEEE Wireless Communications and Networking Conference (WCNC'11)*, 2011.

[7] "D6.1 - First feedback on implementation aspects connected to the selected innovations," *ARTIST 4G technical document*.

[8] M. Grieger, P. Marsch, and G. Fettweis, "Large Scale Field Trial Results on Uplink CoMP with Multi Antenna Base Stations," *IEEE Vehicular Technology Conference (VTC fall)*, 2011.

[9] M. Grieger, P. Helbing, P. Marsch, and G. Fettweis, "Field Trial Evaluation of Compression Algorithms for Distributed Antenna Systems," *Sarnoff Symposium (Sarnoff'11)*, 2011.

[10] M. Grieger, G. Fettweis, and P. Marsch, "Large Scale Field Trial Results on Time Domain Compression for Uplink Joint Detection," *22nd IEEE Personal Indoor Mobile Radio Communications (PIMRC'11 - WACC)*, Toronto, Canada: 2011, pp. 1630-1634.

[11] J. Niemela and J. Lempiainen, "Impact of mechanical antenna downtilt on performance of WCDMA cellular network," *Vehicular Technology Conference, 2004. VTC 2004-Spring. 2004 IEEE 59th*, 2004.

[12] L. Thiele, T. Wirth, M. Schellmann, Y. Hadisusanto, and V. Jungnickel, "MU-MIMO with Localized Downlink Base Station Cooperation and Downtilted Antennas," *2009 IEEE International Conference on Communications Workshops*, IEEE, 2009, pp. 1-5.

[13] "D2.2 Advanced receiver signal processing techniques: evaluation and characterization", ARTIST4G technical deliverable," *ARTIST 4G technical document to appear*, 2011.

[14] 3GPP, 3GPP TS 36.101 V9.2.0 (2009-12) Evolved universal terrestrial radio access (E-UTRA); User equipment (UE) radio transmission and reception, 2009.

[15] Alamouti, S.M., "A simple transmit diversity technique for wireless communications", *Selected Areas in Communications, IEEE Journal on*, Oct 1998, Issue:8, On page(s): 1451 – 1458.

[16] 3GPP TR 25.996 V9.0.0 (2009-12)

[17] 3GPP TR 36.814 V9.0.0 (2010-03)

[18] "D1.2 Innovative advanced signal processing algorithms for interference avoidance", *ARTIST4G technical deliverable,* January, 2011.

[19] P. Marsch; G. P. Fettweis, "Coordinated Multi-Point in Mobile Communications: From Theory to Practice", Cambridge University Press, 2011

[20] "D6.1 First feedback on implementation aspects connected to the selected innovations," *ARTIST 4G technical document,* March, 2011.

[21] A. Hottinen, "Multiuser scheduling with matrix approximation," IEEE International Symposium on Signal Processing and Information Technology ISSPIT 2003, Darmstadt, Germany, 14-17 Dec. 2003.

[22] 3GPP, 3GPP TS 36.521-1 V9.4.1 (2011-03) Evolved universal terrestrial radio access (E-UTRA); User equipment (UE) conformance specification radio transmission and reception, Part 1: Conformance testing, 2009.

[23] "D5.1 Scenarios, Key Performance Indicators and Evaluation Methodology for Advanced Cellular Systems", *ARTIST 4G technical document,* June, 2010.

Abbreviations

ADC	Analogue to Digital Converter
ARQ	Automatic Repeat Request
ASIC	Application Specific Integrated Circuit
AWGN	Additive White Gaussian Noise
BER	Bit Error Rate
BLER	Block Error Rate
BS	Base Station
CFO	Carrier Frequency Offset
CoMP	Coordinated Multi Point
CPU	Central Processing Unit
CRC	Cyclic Redundancy Check
CSI	Channel State Information
DAC	Digital to Analogue Converter
DeNodeB	Donor LTE Base Station
DL	Downlink
DSP	Digital Signal Processor
eNodeB	LTE Base Station
FDD	Frequency Division Duplex
FFT	Fast Fourier Transform
FPGA	Field-Programmable Gate Array
GUI	Graphical User Interface
HARQ	Hybrid Automatic Repeat Request
iFFT	inverse Fast Fourier Transform
JD	Joint Detection
JT	Joint Transmission
L1 / L2	Layer 1 / Layer 2
LTE	Long Term Evolution
LVDS	Low-Voltage Differential Signaling
MAC	Media Access Control
MAC	Multiply ACcumulate
MCS	Modulation and Coding Scheme
MER	Modulation Error Rate
MIMO	Multiple Input Multiple Output
MISO	Multiple Input Single Output
NoC	Network On Chip
OFDM	Orthogonal Frequency Division Multiplexing
PER	Packet Error Rate
PRB	Physical Resource Block
QAM	Quadrature Amplitude Modulation
RAM	Random Access Memory
RISC	Reduced Instruction Set Computer
RN	Relay Node
RRH	Remote Radio Head
RSSI	Receive Signal Strength
Rx	Receiver
SIC	Successive Interference Cancellation
SINR	Signal-to-Interference-and-Noise Ratio

SME	Smart Memory Engine
SDRAM	Synchronous Dynamic Random Access Memory
SOC	System On Chip
SOCIR	Signal-to-Outer-Cell-Interference Ratio
SRAM	Static Random Access Memory
TB	Transport Block
TBS	Transport Block Size
TDD	Time Division Duplex
TTI	Transmit Time Interval
Tx	Transceiver
UE	LTE Terminal
UL	Uplink
VLIW	Very Long Instruction Word